Indoor Point-to-Point Navigation with Deep Reinforcement Learning and Ultra-Wideband

Indoor Point-to-Point Navigation with Deep Reinforcement Learning and Ultra-Wideband

Enrico Sutera[1,2][a], Vittorio Mazzia[1,2,3][b], Francesco Salvetti[1,2,3][c], Giovanni Fantin[1,2][d] and Marcello Chiaberge[1,2][e]

[1]*Department of Electronics and Telecommunications, Politecnico di Torino, 10124 Turin, Italy*

[2]*PIC4SeR, Politecnico di Torino Interdepartmental Centre for Service Robotics, Turin, Italy*

[3]*SmartData@PoliTo, Big Data and Data Science Laboratory, Turin, Italy*

Keywords: Indoor Autonomous Navigation, Autonomous Agents, Deep Reinforcement Learning, Ultra-Wideband.

Abstract: Indoor autonomous navigation requires a precise and accurate localization system able to guide robots through cluttered, unstructured and dynamic environments. Ultra-wideband (UWB) technology, as an indoor positioning system, offers precise localization and tracking, but moving obstacles and non-line-of-sight occurrences can generate noisy and unreliable signals. That, combined with sensors noise, unmodeled dynamics and environment changes can result in a failure of the guidance algorithm of the robot. We demonstrate how a power-efficient and low computational cost point-to-point local planner, learnt with deep reinforcement learning (RL), combined with UWB localization technology can constitute a robust and resilient to noise short-range guidance system complete solution. We trained the RL agent on a simulated environment that encapsulates the robot dynamics and task constraints and then, we tested the learnt point-to-point navigation policies in a real setting with more than two-hundred experimental evaluations using UWB localization. Our results show that the computational efficient end-to-end policy learnt in plain simulation, that directly maps low-range sensors signals to robot controls, deployed in combination with ultra-wideband noisy localization in a real environment, can provide a robust, scalable and at-the-edge low-cost navigation system solution.

1 INTRODUCTION

The main focus of service robotics is to assist human beings, generally performing dull, repetitive or dangerous tasks, as well as household chores. In most of the applications, the robot has to navigate in an unstructured and dynamic environment, thus requiring robust and scalable navigation systems. In practical application, robot motion planning in dynamic environments with moving obstacles adopts a layered navigation architecture where each block attempts to solve a particular task. In a typical stack, in a GPS-denied scenario, precise indoor localization is always a challenging objective with a great influence on the overall system and correct navigation (Rigelsford, 2004). Indeed, algorithms such as SLAM (Cadena et al., 2016) or principal indoor localization techniques based on technologies, such as WiFi, radio frequency identification device (RFID), ultra-wideband (UWB) and Bluetooth (Zafari et al., 2019), are greatly affected by multiple factors; among others, presence of multi-path effects, noise and characteristics of the specific indoor environment are still open challenges that can compromise the entire navigation stack.

Robot motion planning in dynamic and unstructured environments with moving obstacles has been studied extensively (Mohanan and Salgoankar, 2018), but, being an NP-complete (Barraquand and Latombe, 1991) problem, classical solutions have significant limitations in terms of computational request, power efficiency and robustness at different scenarios. Moreover, currently available local navigation systems have to be tuned for each new robot and environment (Chen et al., 2015) constituting a real challenge in presence of dynamical and unstructured environments.

Deep learning and in particular Deep reinforce-

[a] https://orcid.org/0000-0001-5655-3673
[b] https://orcid.org/0000-0002-7624-1850
[c] https://orcid.org/0000-0003-4744-4349
[d] https://orcid.org/0000-0002-9361-3484
[e] https://orcid.org/0000-0002-1921-0126

Sutera, E., Mazzia, V., Salvetti, F., Fantin, G. and Chiaberge, M.
Indoor Point-to-Point Navigation with Deep Reinforcement Learning and Ultra-Wideband.
DOI: 10.5220/0010202600380047
In *Proceedings of the 13th International Conference on Agents and Artificial Intelligence (ICAART 2021) - Volume 1*, pages 38-47
ISBN: 978-989-758-484-8

ment learning (RL) has shown very promising results in fields as diverse as video games (Mnih et al., 2015; Mnih et al., 2013), energy usage optimization (Mocanu et al., 2018), remote sensing (Salvetti et al., 2020; Khaliq et al., 2019; Mazzia et al., 2020) and visual navigation (Zhu et al., 2017; Tamar et al., 2016; Aghi et al., 2020), since 2013. Greatly inspired by the work of Chiang et al. (Chiang et al., 2019), we exploited deep reinforcement learning to obtain an agent robust to localization noise and able to map raw noisy low-level 2-D lidar observations to robot controls linear and angular velocities. Indeed, the obtained learnt policy through a plain and fast simulation process is a light-weight, power-efficient motion planning system that can be deployed at the edge, on very low-cost hardware with limited computational capabilities.

In particular, we focused our research on a tight integration between the point-to-point local motion planner, learnt in simulation, with UWB localization technology, providing experimental proofs of the feasibility of the system UWB-RL in a real setting. UWB radios are rapidly growing in popularity, offering decimeter-level accuracy and increasingly smaller and cheaper transceivers (Magnago et al., 2019). In comparison with other techniques, UWB enables both distance estimation and communication among devices within the same radio chip with relative low-level consumption. However, the accurate estimation of the position of a robot is critical for its correct navigation and, as previously mentioned, also UWB, in a real scenario, is affected by several factors of disturbance. Our results show that, even in the presence of very uncertain localization information, due to the presence of moving obstacles in the environment, multi-path effects and other sources of noise, our proposed solution is robust and has comparable performance with classical approaches. Nevertheless, our solution has a much lower computational request and power consumption constituting a competitive and end-to-end local motion planner solution for indoor autonomous navigation in dynamic and unknown environments.

2 PROPOSED METHOD

2.1 Reinforcement Learning

Deep RL is a machine learning technique that merges deep learning and reinforcement learning together. The latter is generally used for tackling problems that can be modeled as a Markov decision process (MDP). Hence, the typical learning setup consists of an agent which interacts with an environment. The agent selects an action $a_t \in \mathcal{A}$ and performs it in the environment, which gives back a new state $s_{t+1} \in \mathcal{S}$ and a reward r_{t+1}, sequentially at each time-step t. The environment may also be stochastic. $\mathcal{A}$ and $\mathcal{S}$ are the space of the actions and the space of the states, respectively. The reward r_t is the feedback signal at the basis of the learning process from raw data, hence being higher for "better" actions and lower for "worse" ones. The agent chooses an action by following a policy π that maps states to actions. A sequence with shape $s_0, a_0, r_1, s_1, a_1, \ldots, s_i, a_i, r_{i+1}, s_{i+1}$ is then generated, which can be seen as many transitions one after another. The training phase aims at making the agent learn to maximize the return G, which is usually the discounted sum of future rewards, expressed as

$$G = \sum_{k=0} \gamma^k R_{t+k+1} \tag{1}$$

The term γ is called discount factor and it regulates the importance of rewards along the episode. It can assume values between 0 (only the immediate reward is important) and 1 (all future rewards are equally important). The agent is typically characterized by a policy $\pi(a|s)$ which maps states to actions. A policy can be stochastic, e.g. can give the probability of an ac-

Algorithm 1: DDPG algorithm.

Initialization of critic and actor networks:
$Q(s,a|\theta^Q)$, $Q'(s,a|\theta^{Q'})$, $\mu(s,a|\theta^\mu)$, $\mu'(s,a|\theta^{\mu'})$
Initialization of replay memory $\mathcal{D}$
for *episode in M* **do**
  Receive initial state s_1 **for** *iteration t in T* **do**
    Generate random number $0 \leq h \leq 1$
    if $h \leq \varepsilon$ **then**
      Select a random action a_t
    end
    else
      Select $a_t = \mu(s_t, \theta^\mu)$;
    end
    Execute action a_t and receive r_t, s_{t+1}
    Store transition (s_t, a_t, r_t, s_{t+1}) in $\mathcal{D}$
    Sample a random mini-batch of transitions (s_j, a_j, r_j, s_{j+1}) from replay memory $\mathcal{D}$
    Set target: $y_j =$
    $\begin{cases} 1 : r_j \quad if\, final state \\ 0 : r_j + \gamma Q'(s_{j+1}, \mu'(s_{j+1}|\theta^{\mu'})|\theta^{Q'}) \end{cases}$
    Update critic minimizing loss:
    $L = (y_i - Q(s_j, a_j \theta^Q))^2)$
    Update μ using the policy gradient: $\Delta_{\theta^\mu} J \approx \Delta_a Q(s,a,|\theta^Q)|_{s_j, \mu(s_j)} \Delta_{\theta^\mu} \mu(s|\theta^\mu)|_{s_j}$
    if $global step \,\%\, update step == 0$ **then**
      $\theta^{Q'} \leftarrow \theta^Q$, $\theta^{\mu'} \leftarrow \theta^\mu$
    end
  end
end

tion a to be taken when in state s, or deterministic, hence giving the action directly and in this case is often denoted by μ.

Since the aim of an agent is to maximise G, it is useful to define the expected return when an action a_t is taken from a state s_t and then a policy π is followed. This is expressed by the action-value function:

$$Q^{\pi}(s_t, a_t) = \mathbb{E}_{r_{i\geq t}, s_{i>t} \sim E, a_{i>t} \sim \pi}[R_t \mid s_t, a_t] \quad (2)$$

In many RL approaches the Bellman equation is used:

$$\begin{aligned} Q^{\pi}(s_t, a_t) = \mathbb{E}_{r_t, s_{t+1} \sim E}[r(s_t, a_t) \\ + \gamma \mathbb{E}_{a_{t+1} \sim \pi}[Q^{\pi}(s_{t+1}, a_{t+1})]] \end{aligned} \quad (3)$$

which, under target deterministic policy becomes:

$$\begin{aligned} Q^{\mu}(s_t, a_t) = \mathbb{E}_{r_t, s_{t+1} \sim E}[r(s_t, a_t) \\ + \gamma[Q^{\mu}(s_{t+1}, a_{t+1})]] \end{aligned} \quad (4)$$

This relationship is used to learn Q^{μ} off policy, that means that the exploited transition can also be generated by using another stochastic behavioural policy β. This approach can be referred to as Q-learning. Considering a finite action space, once the Q function is known, it is sufficient to choose the action that maximizes the expected returns. This is also called greedy policy:

$$\mu(s) = argmax_a Q(s, a) \quad (5)$$

If we consider to approximate the action-value function using a function approximator, whose parameters can be denoted as θ^Q, the optimization can be performed by minimizing the loss, which can be expressed as:

$$L(\theta^Q) = \mathbb{E}_{s_t \sim \rho^{\beta}, a_t \sim \beta, r_t \sim E}[(Q(s_t, a_t \mid \theta^Q) - y_t)^2] \quad (6)$$

where:

$$y_t = r(s_t, a_t) + \gamma Q(s_{t+1}, \mu(s_{t+1} \mid \theta^Q)) \quad (7)$$

and ρ denotes the discounted state visitation distribution for a policy β. This procedure was recently used along with two new feature: a *replay buffer* and a *target network* for obtaining the target y_t (Mnih et al., 2013)(Mnih et al., 2015).

2.2 Deep Deterministic Policy Gradient

The above seen Q-learning-related procedure cannot be directly applied to a problem with a continuous action space. So, we implement a version of the deep deterministic policy gradient (DDPG) algorithm (Lillicrap et al., 2015) that uses an actor-critic approach to overcome the limitations of discrete actions. Considering to be using function approximators, actor and critic can be denoted respectively as $\mu(s \mid \theta^{\mu})$ and $Q(s, a \mid \theta^Q)$. The critic function is learned as done in Q-learning, hence using the Bellman equation and exploiting the same loss. The actor function instead is updated by exploiting the knowledge of the policy gradient (Silver et al., 2014). Considering a starting distribution $J = \mathbb{E}_{r_i, s_i \sim E, a_i \sim \pi}[R_1]$ and applying the chain rule to the expected return with respect to the parameters of the actor, the policy gradient can be obtained:

$$\begin{aligned} \Delta_{\theta^{\mu}} J &\approx \mathbb{E}_{s_t \sim \rho^{\beta}}[\Delta_{\theta^{\mu}} Q(s, a \mid \theta^Q) \mid_{s=s_t, a=\mu(s_t \mid \theta^{\mu})}] \\ &= \mathbb{E}_{s_t \sim \rho^{\beta}}[\Delta_a Q(s, a \mid \theta^Q) \mid_{s=s_t, a=\mu(s_t)} \\ &\quad \cdot \Delta_{\theta^{\mu}} \mu(s \mid \theta^{\mu}) \mid_{s=s_t}] \end{aligned} \quad (8)$$

The full pseudo-code is shown in Alg. 1. We hardly update the target networks periodically instead of performing a continuous soft update. Moreover, we tackle the exploration-exploitation dilemma by maintaining an ε probability to perform a random action rather than following the policy μ. The value of epsilon decays during the training as:

$$\varepsilon = \max(\varepsilon_0 \varepsilon_d^{episode}, \varepsilon_{min}) \quad (9)$$

where ε_d is the decay parameter.

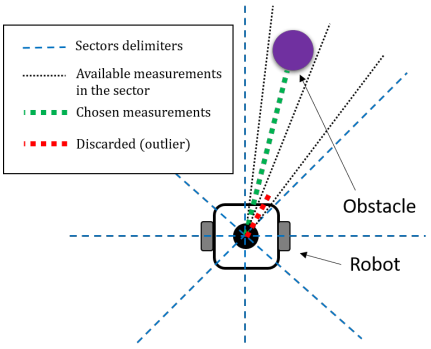

Figure 1: Scheme of used lidar measurements. Lower values of distance are considered more significant for obstacle detection.

2.3 Point-to-Point Agent Training

In this work, we deal with continuous domains, holding $\mathcal{A} \in \mathbf{R}^N$ (continuous control) and $\mathcal{S} \in \mathbf{R}^M$ (continuous state space), with N and M dimensions of action and observation spaces. Concerning the latter, the observation is the representation that the agent has of the current state. In our case, the observation is a vector with 62 elements. It is made of 60 1-D measurements of the lidar, and distance and angle with respect to the goal. During the simulation phase, we use odometry data and magnetometer measurements

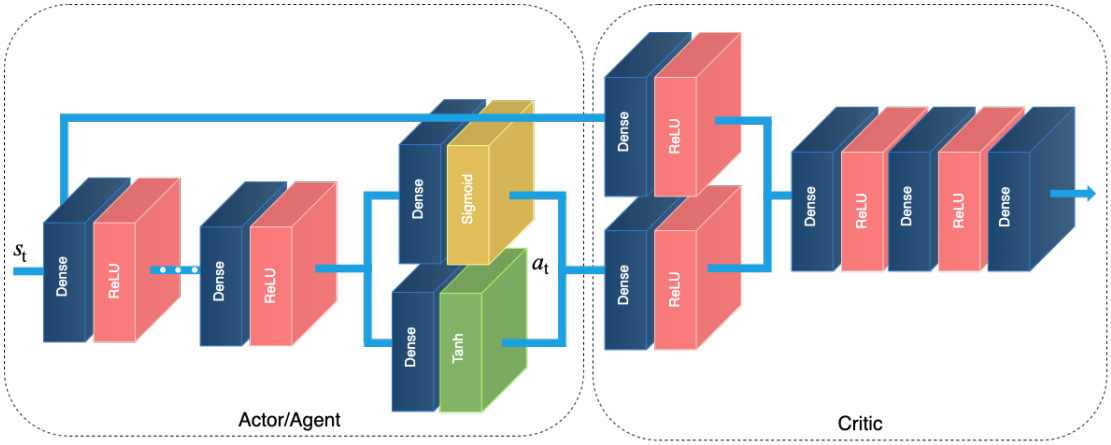

Figure 2: Graphical representation of the actor/critic architecture. During the training procedure, the actor processes the observations of the robot s_t with a cascade of fully connected layers producing distinct actions a_t for the angular and linear velocity. Subsequently, the critic network takes as input both s_t and a_t generating the corresponding Q value estimation. After the training procedure, the policy learnt by the agent in simulation is exploited by the robot to navigate from point-to-point.

to compute and provide the previously mentioned distance and angle. This clearly demonstrates the robustness of the trained agent, which is able to generalize to the real scenario even without explicitly modelling UWB localization signals during the training process. The 1-D 60 measurements are not equally spaced. Instead, the whole 2π circle is split into 60 sectors, and the minimum non-outliers are taken, to guarantee the knowledge of nearer obstacles, as shown in Fig. 1.

The action instead is a 2-D vector, containing the angular and the linear velocity of the robot:

- Linear velocity: the *sigmoid* activation function guarantees a value between 0 and 1 since we want the robot to only have non-negative values of speed;
- Angular velocity: the *hyperbolic tangent* activation function constraints the output between -1 and 1.

According to the *target network* technique, we use four networks: actor network, critic network and their target twins, with the same architectures represented in Fig. 2. The networks are mainly constituted by fully connected layers with ReLU activation functions, except for the final ones. The first three layers of the actor have respectively 512, 256 and 256 neurons. The critic first two hidden layers have respectively 256 (state side) and 64 (action side) units. The following hidden layers have 256 and 128 neurons sequentially. The last layer of the critic is a single output FC with linear activation function to provide the Q value.

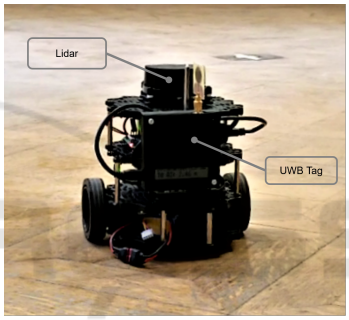

Figure 3: The robotic platform used for the experimentation: a Robotis TurtleBot3 Burger with a Decawave EVB1000 Ultra-wideband tag.

3 EXPERIMENTAL DISCUSSION AND RESULTS

In this section, we present the hardware and software setup used during the experimentation phase. We provide a full description of the training phase of the RL agent, with a detailed list of all the selected hyperparameters. Finally, we describe the different tests performed and we present a quantitative evaluation of the proposed local planner.

3.1 Hardware and Robotic Platform

The training of the RL agent is performed using a workstation with an Intel Core i7 9700k CPU, along with 64 GB of RAM. It takes around 24 hours to complete. Concerning the robotic platform, we select the

Table 1: Adopted hyperparameters in simulation during the point-to-point agent training.

Hyper-parameters	
starting epsilon	1
minimum epsilon	0.05
epsilon decay	0.998
learning rate	0.00025
discount factor	0.99
sample size	64
batch size	64
target network update	2000
deque memory maxlen	1000000

Robotis TurtleBot3 Burger model[1], which is a low-cost, ROS-oriented (Robot Operating System) solution. An accurate model is also provided for Gazebo simulations. The Turtelbot3 Burger model we use is equipped with a Raspberry Pi 3 B+. Concerning the Ultra-wideband hardware, we use a TREK1000 evaluation kit by Decawave to provide the agent with the localization data that in simulation are obtained via odometry and magnetometer measurements. Fig. 3 shows the complete robotic platform used during the experimentation.

3.2 RL Agent Training

The training is performed simulating both agent and environment on Gazebo. The robot is controlled by the actor network presented in the methodology. The training is performed in episodes, that means the robot is re-spawned in the same starting point. The objective for each episode is to reach a randomly spawned goal and the reward that is given to the agent depends on it. We use the following equation to provide reward values:

$$R = \begin{cases} +1000, & \text{if goal is reached} \\ -200, & \text{if collision occurs} \\ 3 \cdot h_R \cdot 10 \cdot |\Delta d|, & \text{else,} \end{cases} \quad (10)$$

where Δd is the difference between distance at current and previous instants of time, and:

$$h_R = -\left(\omega_{t-1} \cdot \frac{1}{1.2 \cdot f} - heading\right)^2 + 1 \quad (11)$$

is the heading reward. ω is the angular speed, while f is the control frequency. The third part of the equation gives a positive reward when the robot is getting closer to the goal ($|\Delta d|$ contribute). Moreover, this value is higher if it is directly pointing it (h_R contribute). The values of the hyperparameters used in the training phase are shown in Tab. 1. The *target network update* sets how often the target networks are hardly updated, in terms of steps. The same value of learning rate is used for both actor and critic, equal to 0.00025. The discount factor is set to a value of 0.99, as for the epsilon decay. Tab. 2 presents the environment and the robot settings used in simulation.

[1] http://www.robotis.us/turtlebot-3/

Table 2: Selected settings of the robot and of the simulated environment during the training of the deep reinforcement learning agent.

Robot settings	
lidar points	60
ctrl period	0.33
maximum angular speed	$1 rad/s$
maximum linear speed	$0.2 m/s$
Simulation settings	
time step	$0.0035 s$
max update rate	$2000 s^-1$
timeout	$250 s$ (in sim. time)

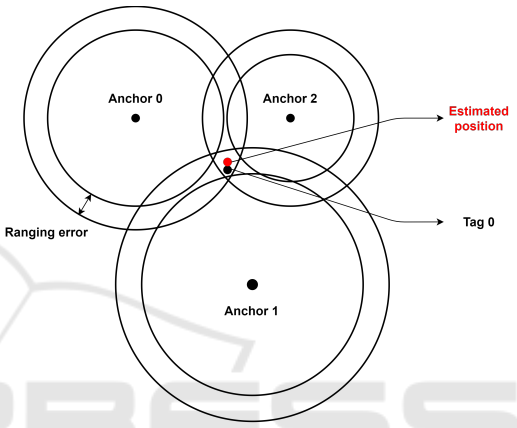

Figure 4: Estimation of the position in the x-y plan using error affected ranging measurements.

3.3 Ultra-Wideband Settings

In our experimental setup, we use UWB as the only positioning method, do its robustness against the noise in the localization measurements. The real-time locating system (RTLS) is composed of 5 Decawave EVB1000 boards: 4 placed in fixed positions (anchors) at the corners of the experimental area and one mounted on the robotic platform. The EVB1000 boards are set to communicate using channel 2 (central frequency 3.993 GHz) with a data rate of 6.8 Mbps, a preamble length of 128 symbols and a positioning update rate of 10 Hz. We mount the four anchors on four tripods at slightly different heights, with maximum height set at less than 2 meters. The position of the anchors along the vertical axis strongly affects the precision of the localization in the hor-

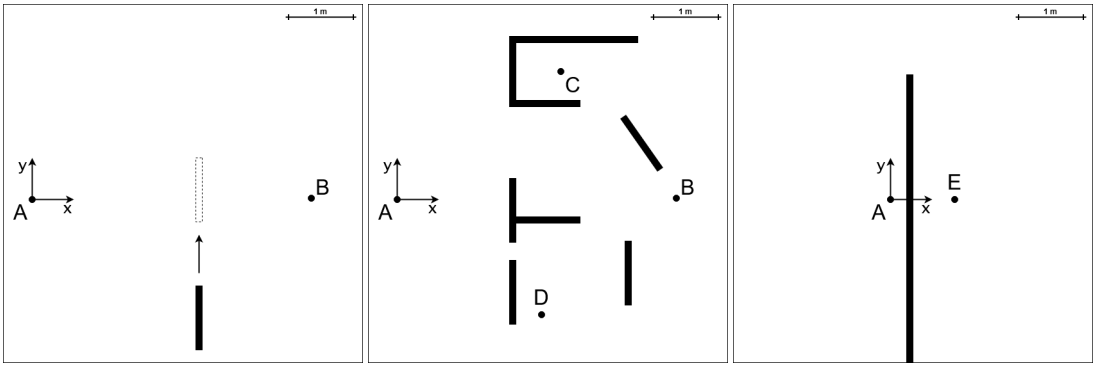

(a) Path: *AB*. (b) Path: *ABCD*. (c) Path: *AE*.

Figure 5: Scenarios used in the first set of tests for the local planner evaluation. Points positions: $A(0,0)$ m, $B(4.35,0.02)$ m, $C(2.55,2)$ m, $D(2.25,-1.8)$ m, $E(1,0)$ m.

izontal (x-y) plan, increasing the height is possible to achieve better performances. Moreover, the robot (target) is able to move outside the area defined by the fixed devices, and this is a critical situation for the computation of the position. The raw ranging data are smoothed using a simple linear Kalman filter. The measurement noise covariance, computed in previous experiments, is set to $\sigma_m^2 = 6.67 * 10^{-4}$ and the process noise covariance ($\sigma_p^2 = 10^{-4}$) is chosen to obtain the desired behavior from the filter. Finally, the position of the robot is computed as the intersection of the four spheres centered in the anchors' positions with a radius equal to the corresponding ranging measurements, as schematically shown in Fig. 4. This is a typical nonlinear estimation problem that we solve using the Gauss-Newton nonlinear least-squares method, which is a well-suited algorithm for range-based position estimation, as discussed in (Yan et al., 2008). At each sampling step, the new position is estimated starting the iteration from the last known point.

3.4 Experimental Settings

To prove the robustness and the reliability of the proposed system, we perform several experimentations that can be grouped into two test sets. In the first, we compare our system with a classical one based on the well-known Dynamic Window Approach (DWA) (Fox et al., 1997) in different scenarios to prove that our local planner achieves better performances, with lower computational effort. In the second set of tests, we focus on the robustness of the system to UWB localization noise, and we compare it to the performance obtained by humans put in the same testing conditions of the RL agent. The achieved results thoroughly show how the proposed system can represent a reliable and efficient local planner to enable autonomous navigation in unknown and unstructured environments.

In all the following tests, we fix the reference frame on the initial position of the robot and measure the positions with a Leica AT403 Laser Tracker. The main metric for navigation performance is the success rate. Each experiment is considered successful if the robot is able to get within 20 cm to the target position without getting stuck. Since the robot can theoretically reach the goal also with random wandering, we consider a maximum time $t_{\max}$. If the robot is unable to reach the target position within this time interval, the test is considered failed. Considering the maximum linear speed of $0.22\,\mathrm{m\,s^{-1}}$ of the Turtlebot3 Burger and an average path length of 5.5 m over all the experiments, we consider 180 s as a reasonable value for $t_{\max}$. Moreover, we consider the mean total time t^{mean} as a metric to understand how well the local planner is able to find an optimal solution to the navigation problem and RMS accelerations $\dot{v}^{\mathrm{RMS}}$, $\dot{\omega}^{\mathrm{RMS}}$ as metrics for navigation smoothness. Finally, collisions with static or moving obstacles are registered for each test, since the ability to avoid them assumes a vital relevance in robotic autonomous navigation.

3.5 Local Planner Quantitative Evaluation

The first set of tests is aimed at comparing the proposed local planner with the most used Dynamic Window Approach (DWA) (Fox et al., 1997). We use the ROS implementation of this navigation algorithm, based on the work of Brock et al. (Brock and Khatib, 1999). The two algorithms are compared with repeated tests in three different scenarios:

1. the robot has to navigate to the target point autonomously and is suddenly interrupted by a moving obstacle;

Table 3: Experimental results of the first set of tests: comparison with DWA (Fox et al., 1997) local planner.

Scenario	Algorithm	Success rate	t^{mean} [s]	$\dot{v}^{\text{RMS}}$ [m s^{-2}]	$\dot{\omega}^{\text{RMS}}$ [rad s^{-2}]
S1	DWA	1	37	0.2277	1.1371
	RL+UWB	1	33	0.1342	1.6382
$S2_{AB}$	DWA	0.80	48	0.3016	1.0022
	RL+UWB	1	45	0.1535	2.6922
$S2_{BC}$	DWA	0.70	97	0.2866	1.6434
	RL+UWB	0.91	65	0.1149	1.4719
$S2_{CD}$	DWA	0.50	129	0.2757	0.9180
	RL+UWB	0.91	94	0.1050	1.5483
$S2_{ABCD}$	DWA	0.50	261	0.2880	1.1879
	RL+UWB	0.91	223	0.1225	1.7528
S3	DWA	1	48	0.1920	1.1390
	RL+UWB	1	31	0.1047	1.4132

2. the robot has to navigate to three waypoints in a certain order inside a fairly complex environment;
3. the robot has to reach a goal located behind a wall, with single opening quite far from the goal.

Fig. 5 shows a visual presentation of the first tests set scenarios. The first one is particularly useful to evaluate the obstacle avoidance performance of the algorithm and its ability to react to a sudden change in the navigation environment, by following a new safer path to reach the target. In this case, the moving obstacle consists in a panel put in front of the robot while it is navigating towards the target. The second scenario shows the ability to solve subsequent point-to-point tasks in a quite complex and unstructured environment. The robot starts in point *A* and has to navigate segments *AB*, *BC*, *CD*, subsequently. We evaluate performances both on the single point-to-point tasks and on the whole path *ABCD*. Finally, the last scenario is relevant to judge the ability of the algorithm to adopt local sub-optimal actions that make the robot actually increase the distance from the target, in order to be subsequently able to reach the final goal. In this sense, this kind of situation is useful to evaluate whether the robot is able to escape local minima.

We perform a total of 30 tests for both the algorithms in the three different scenarios. Tab. 3 summarizes the experimentation. In general, our approach has a higher success rate and requires, on average, less time to reach the target. It gets lower linear accelerations, but higher angular ones, resulting in a lower smoothness on the angular control. The second scenario appears to be the toughest one, in particular in its third task *CD*, where the DWA success rate drops to 0.5. In all these tests, we register no collisions with both the algorithms. However, the main advantage of the proposed local planner is its computational effort. We achieve up to 400 Hz control frequency the proposed RL planner. On the other hand, since the DWA is an optimization algorithm, on the same machine it ranges between 0.5 Hz and 5 Hz. This dramatic improvement in computational efficiency allows for the proposed local planner to be completely run in an embedded system on the robot itself, without the need of a powerful machine as classic algorithms as DWA do. We deploy the RL agent on a Raspberry Pi3 B+ embedded computer, and we are able to achieve a real-time control at about 30 Hz.

3.6 Noise Robustness and Human Comparison

The second set of tests is aimed at comparing the proposed algorithm with human performance, as well as demonstrate how the RL+UWB system is highly robust against localization noise. In literature, RL agents are frequently compared to human agents to prove their control performance in complex tasks (Mnih et al., 2015; Silver et al., 2016; Mirowski et al., 2016; Silver et al., 2018). We perform such comparison by putting several people in the same experimental conditions of the RL agent. Human testers are kept in a different room with respect to the experimental environment and can see in real-time the robot position, the goal and the 1-D lidar range measurements, that are exactly the same information available to the RL planner. Fig. 7 presents the interface shown to human testers during the experimentation. Both humans and RL agent are tested in the following scenarios, shown in Fig. 6:

1. the robot has to navigate to the target point autonomously and is suddenly interrupted by a person;
2. the robot has to pass through a small opening partially occluded by a moving obstacle;
3. the robot has to navigate to three waypoints in a certain order inside a fairly complex environment;

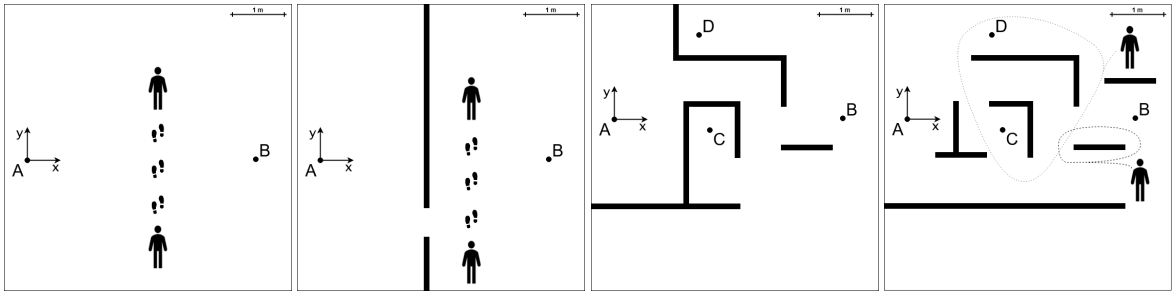

(a) Path: *AB*. (b) Path: *AB*. (c) Path: *ABCD*. (d) Path: *ACBD*.

Figure 6: Scenarios used in the second set of tests for the comparison with human control. Points positions: $A(0,0)$ m, $B(4.45,0.02)$ m, $C(1.86,-0.21)$ m, $D(1.65,1.65)$ m.

Table 4: Experimental results of the second set of tests: comparison with human control.

Scenario	Agent	Success rate	Collisions	t^{mean} [s]	$\dot{v}^{\text{RMS}}$ [m s^{-2}]	$\dot{\omega}^{\text{RMS}}$ [rad s^{-2}]
S1	Human	1	0	30	0.3574	2.0783
	RL+UWB	1	0	29	0.3557	3.8413
S2	Human	1	0.25	42	0.3382	2.0012
	RL+UWB	1	0	50	0.3333	4.5058
$S3_{AB}$	Human	1	0.25	38	1.7703	2.1109
	RL+UWB	1	0	39	0.3513	4.1098
$S3_{BC}$	Human	1	0.50	36	0.3643	2.0638
	RL+UWB	1	0	29	0.3495	4.1354
$S3_{CD}$	Human	0.75	0.25	97	0.3691	2.1878
	RL+UWB	0	0	-	-	-
$S3_{ABCD}$	Human	0.75	1	161	0.3696	2.1490
	RL+UWB	0	0	-	-	-
$S4_{AC}$	Human	1	0	49	0.3227	2.1171
	RL+UWB	1	0	49	0.3230	4.5523
$S4_{CB}$	Human	1	0.25	40	0.3224	2.3882
	RL+UWB	1	0	28	0.3393	4.4387
$S4_{BD}$	Human	1	0	49	0.3420	2.1848
	RL+UWB	1	0	25	0.3280	4.3618
$S4_{ACBD}$	Human	1	0.25	137	0.3290	2.2301
	RL+UWB	1	0	102	0.3301	4.4509

4. the robot has to navigate to three waypoints in a certain order inside a fairly complex environment with both static and moving obstacles (people wandering in the scenario).

In all these tests, Gaussian noise is superimposed to UWB measurements in order to evaluate the robustness of the system to localization errors. Higher uncertainty in the UWB positioning is also caused by the presence of people in the environments (scenarios 1, 2, 4) who obstruct the anchors and cause the NLOS (non-line of sight) condition. Fig. 8 shows an example of the trajectory followed by the robot in the first scenario (path *AB*, interrupted by a sudden moving person). The noisy signal of the UWB clearly gives a high uncertainty on the position of the robot. However, the RL local planner is highly robust against localization errors and it is able to reach the goal.

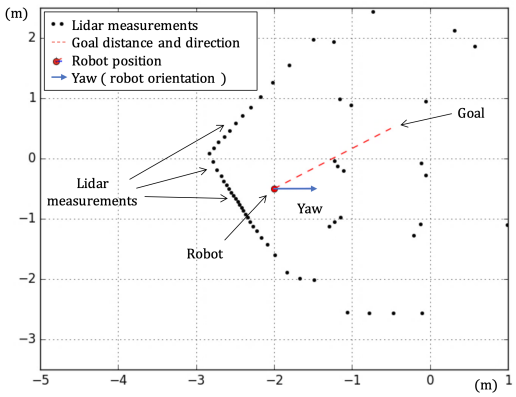

Figure 7: Human interface during the second tests set. Testers are allowed to see lidar measurements, robot pose and goal distance and direction.

Tab. 4 presents the results of the second set of tests. In general, the RL+UWB appears to have similar performances to human control, even in the presence of localization noise. The proposed algorithm appears to be particularly able in avoiding obstacles, while humans result more subject to collisions in complex environments. One interesting thing to notice is that the RL+UWB is completely unable to solve the *CD* task of scenario 3, when the robot is surrounded by walls on three edges. It remains stuck, repeating the same actions over and over. This behavior can be explained by the absence of memory in this kind of planners, that makes them unable to escape from too narrow local minima. Humans are able to analyze subsequent states and can understand how the environment is actually disposed, while the RL agent simply reacts to the current state and cannot build an environment map.

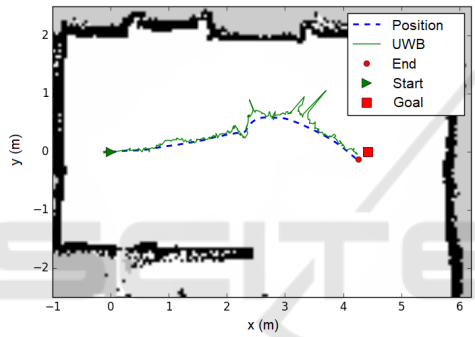

Figure 8: Trajectory followed in a test in the first scenario (path *AB*, interrupted by a sudden moving person). The UWB added noise is clearly visible and shows how the proposed local planner is highly robust against positioning errors.

4 CONCLUSION

In this paper, we proposed a novel indoor local motion planner based on a strict synergy between an autonomous agent trained with deep reinforcement learning and ultra-wideband localization technology. Indoor autonomous navigation is a challenging task, and localization techniques can generate noisy and unreliable signals. Moreover, due to the high complexity of typical environments, hand-tuned classical methodologies are highly prone to failure and require access to a large number of computational resources. The extensive experimentation and evaluations of our research proved that our low-cost and power-efficient solution has comparable performance with classical methodologies and is robust to noise and scalable to dynamic and unstructured environments.

ACKNOWLEDGEMENTS

This work has been developed with the contribution of the Politecnico di Torino Interdepartmental Centre for Service Robotics PIC4SeR[2] and SmartData@Polito[3]. This work is partially supported by the Italian government via the NG-UWB project (MIUR PRIN 2017).

REFERENCES

Aghi, D., Mazzia, V., and Chiaberge, M. (2020). Local motion planner for autonomous navigation in vineyards with a rgb-d camera-based algorithm and deep learning synergy. *Machines*, 8(2):27.

Barraquand, J. and Latombe, J.-C. (1991). Robot motion planning: A distributed representation approach. *The International Journal of Robotics Research*, 10(6):628–649.

Brock, O. and Khatib, O. (1999). High-speed navigation using the global dynamic window approach. In *Proceedings 1999 IEEE International Conference on Robotics and Automation (Cat. No. 99CH36288C)*, volume 1, pages 341–346. IEEE.

Cadena, C., Carlone, L., Carrillo, H., Latif, Y., Scaramuzza, D., Neira, J., Reid, I., and Leonard, J. J. (2016). Past, present, and future of simultaneous localization and mapping: Toward the robust-perception age. *IEEE Transactions on robotics*, 32(6):1309–1332.

Chen, C., Seff, A., Kornhauser, A., and Xiao, J. (2015). Deepdriving: Learning affordance for direct perception in autonomous driving. In *Proceedings of the IEEE International Conference on Computer Vision*, pages 2722–2730.

Chiang, H.-T. L., Faust, A., Fiser, M., and Francis, A. (2019). Learning navigation behaviors end-to-end with autorl. *IEEE Robotics and Automation Letters*, 4(2):2007–2014.

Fox, D., Burgard, W., and Thrun, S. (1997). The dynamic window approach to collision avoidance. *IEEE Robotics & Automation Magazine*, 4(1):23–33.

Khaliq, A., Mazzia, V., and Chiaberge, M. (2019). Refining satellite imagery by using uav imagery for vineyard environment: A cnn based approach. In *2019 IEEE International Workshop on Metrology for Agriculture and Forestry (MetroAgriFor)*, pages 25–29. IEEE.

Lillicrap, T. P., Hunt, J. J., Pritzel, A., Heess, N., Erez, T., Tassa, Y., Silver, D., and Wierstra, D. (2015). Continuous control with deep reinforcement learning.

Magnago, V., Corbalán, P., Picco, G., Palopoli, L., and Fontanelli, D. (2019). Robot localization via odometry-assisted ultra-wideband ranging with stochastic guarantees. In *Proc. IEEE/RSJ Int. Conf. Intell. Robots Syst.(IROS)*, pages 1–7.

Mazzia, V., Khaliq, A., and Chiaberge, M. (2020). Improvement in land cover and crop classification based on

[2]https://pic4ser.polito.it

[3]https://smartdata.polito.it

temporal features learning from sentinel-2 data using recurrent-convolutional neural network (r-cnn). *Applied Sciences*, 10(1):238.

Mirowski, P., Pascanu, R., Viola, F., Soyer, H., Ballard, A. J., Banino, A., Denil, M., Goroshin, R., Sifre, L., Kavukcuoglu, K., et al. (2016). Learning to navigate in complex environments. *arXiv preprint arXiv:1611.03673*.

Mnih, V., Kavukcuoglu, K., Silver, D., Graves, A., Antonoglou, I., Wierstra, D., and Riedmiller, M. (2013). Playing atari with deep reinforcement learning. *arXiv preprint arXiv:1312.5602*.

Mnih, V., Kavukcuoglu, K., Silver, D., Rusu, A. A., Veness, J., Bellemare, M. G., Graves, A., Riedmiller, M., Fidjeland, A. K., Ostrovski, G., et al. (2015). Human-level control through deep reinforcement learning. *Nature*, 518(7540):529.

Mocanu, E., Mocanu, D. C., Nguyen, P. H., Liotta, A., Webber, M. E., Gibescu, M., and Slootweg, J. G. (2018). On-line building energy optimization using deep reinforcement learning. *IEEE Transactions on Smart Grid*.

Mohanan, M. and Salgoankar, A. (2018). A survey of robotic motion planning in dynamic environments. *Robotics and Autonomous Systems*, 100:171–185.

Rigelsford, J. (2004). Introduction to autonomous mobile robots. *Industrial Robot: An International Journal*.

Salvetti, F., Mazzia, V., Khaliq, A., and Chiaberge, M. (2020). Multi-image super resolution of remotely sensed images using residual attention deep neural networks. *Remote Sensing*, 12(14):2207.

Silver, D., Huang, A., Maddison, C. J., Guez, A., Sifre, L., Van Den Driessche, G., Schrittwieser, J., Antonoglou, I., Panneershelvam, V., Lanctot, M., et al. (2016). Mastering the game of go with deep neural networks and tree search. *nature*, 529(7587):484.

Silver, D., Hubert, T., Schrittwieser, J., Antonoglou, I., Lai, M., Guez, A., Lanctot, M., Sifre, L., Kumaran, D., Graepel, T., et al. (2018). A general reinforcement learning algorithm that masters chess, shogi, and go through self-play. *Science*, 362(6419):1140–1144.

Silver, D., Lever, G., Heess, N., Degris, T., Wierstra, D., and Riedmiller, M. (2014). Deterministic policy gradient algorithms. In *Proceedings of the 31st International Conference on International Conference on Machine Learning - Volume 32*, ICML'14, page I–387–I–395. JMLR.org.

Tamar, A., Wu, Y., Thomas, G., Levine, S., and Abbeel, P. (2016). Value iteration networks. In *Advances in Neural Information Processing Systems*, pages 2154–2162.

Yan, J., Tiberius, C., Bellusci, G., and Janssen, G. (2008). Feasibility of gauss-newton method for indoor positioning. In *2008 IEEE/ION Position, Location and Navigation Symposium*, pages 660–670.

Zafari, F., Gkelias, A., and Leung, K. K. (2019). A survey of indoor localization systems and technologies. *IEEE Communications Surveys & Tutorials*.

Zhu, Y., Mottaghi, R., Kolve, E., Lim, J. J., Gupta, A., Fei-Fei, L., and Farhadi, A. (2017). Target-driven visual navigation in indoor scenes using deep reinforcement learning. In *2017 IEEE international conference on robotics and automation (ICRA)*, pages 3357–3364. IEEE.